Variable Phase PPM Undulator Study

Zachary Wolf
SLAC

May 17, 2011

Abstract

The LCLS-II undulators will have adjustable K values. One method to change K is to move one row of magnets longitudinally past the other row, i.e. vary the phase of the undulator. In this note we study the variable phase undulator concept to see if it is indeed a possible candidate for the LCLS-II undulators.

1 Introduction[1]

A variable phase undulator changes its K value by moving its upper row of magnets longitudinally relative to its lower row[2]. When opposite poles are vertically aligned, the K value is maximum. When like poles are vertically aligned, the K value is zero. All intermediate K values are available.

The variable phase design might be useful for LCLS-II. The design is compact, so it may be possible to build adjustable K undulators with a size similar to the the fixed K undulators of LCLS-I. This would allow many of the techniques used to build LCLS-I to be used for LCLS-II. For instance, the undulators could be mounted on girders along with the quadrupoles so the undulator-to-quadrupole alignment could be done with high accuracy on a CMM. The undulators could also have a magnetic shield placed around them to reduce the field integral sensitivity to external fields.

In this note, a pure permanent magnet (PPM) variable phase undulator is studied. The undulator was simulated using a charge model for the magnets. Details of the model and end design are given. The undulator fields are calculated. The forces on the magnet arrays are calculated. An analysis program was used to track particles through the field. The K value and the particle trajectories are calculated. Results of the calculations under various undulator configurations are given.

2 PPM Undulator Model

This section describes the model of the undulator that was constructed for this study. The magnetic field was calculated, and trajectories, phase, magnetic forces, etc. were calculated using the magnetic field along a line, similar to the way an undulator is measured along a line and the beam properties are calculated from the measurements. To calculate the fields, a charge model of the magnetic material was used. Details of the model will be presented. The ends of the undulator were designed to be steering free and give a trajectory centered on the beam axis, as will be discussed below. Since the field along a line is used for the trajectory and phase, small changes in the field at the actual electron position are not included. The forces were calculated by assuming the calculated fields are uniform over the width of the undulator. Details of the force calculation will be presented.

[1] Work supported in part by the DOE Contract DE-AC02-76SF00515. This work was performed in support of the LCLS project at SLAC.

[2] R. Carr, "Adjustable Phase Insertion Devices As X-Ray Sources", Nucl. Instr. Meth. A 306 (1991) 391.

2.1 Charge Model

Rare earth permanent magnet materials have an approximately linear B-H curve in the second quadrant[3] which can be expressed as

$$\mathbf{B} = \mu_0 \mathbf{H} + \mathbf{B}_r \tag{1}$$

In this and the following expressions, we use bold font to indicate a vector. We assume $\mu \approx \mu_0$ for both the parallel and perpendicular block magnetization directions. Outside the block, $\mathbf{B}_r = 0$, so equation 1 can be used at all locations with our approximations.

The fields obey the equations

$$\nabla \times \mathbf{H} = 0 \tag{2}$$

$$\nabla \cdot \mathbf{B} = 0 \tag{3}$$

Inserting equation 1 into equation 3, we find

$$\nabla \cdot \mathbf{H} = -\frac{1}{\mu_0} \nabla \cdot \mathbf{B}_r \tag{4}$$

We define the magnetic volume charge density as $\rho_m \equiv -\frac{1}{\mu_0} \nabla \cdot \mathbf{B}_r$. Equations 2 and 4 have the same form as the equations of electrostatics.

$$\nabla \times \mathbf{H} = 0 \tag{5}$$

$$\nabla \cdot \mathbf{H} = \rho_m \tag{6}$$

The solution for $\mathbf{H}$ is derived in an analogous manner to electrostatics by using the magnetic scalar potential ϕ_m, where $\mathbf{H} = -\nabla \phi_m$.

$$\nabla^2 \phi_m = -\rho_m \tag{7}$$

Using standard techniques, one solves for ϕ_m.

$$\phi_m(\mathbf{x}) = \frac{1}{4\pi} \int \frac{\rho_m(\mathbf{x}')}{|\mathbf{x}' - \mathbf{x}|} dV' \tag{8}$$

In this expression, care must be used at the boundaries of a permanent magnet block where ρ_m is singular. We introduce a surface charge density to deal with the boundaries. The magnetic surface charge density is derived from the magnetic volume charge density using the definition of divergence:

$$\nabla \cdot \mathbf{B}_r = \lim_{V \to 0} \frac{\oint \mathbf{B}_r \cdot d\mathbf{A}}{V} \tag{9}$$

where the integral is over the surface of the volume and $d\mathbf{A}$ is an area element oriented toward the outer normal to the surface. Consider a small volume at the surface of a block. The magnetic charge in the volume is $\rho_m \, dV$. The definition of divergence lets us rewrite the charge at the surface in terms of a surface charge density as follows.

$$\rho_m \, dV = -\frac{1}{\mu_0} \nabla \cdot \mathbf{B}_r \, dV \tag{10}$$

$$= -\frac{1}{\mu_0} \lim_{V \to 0} \oint \mathbf{B}_r \cdot d\mathbf{A} \tag{11}$$

$$= \frac{1}{\mu_0} \mathbf{B}_r \cdot d\mathbf{A} \tag{12}$$

$$= \sigma_m dA \tag{13}$$

[3] K. Halbach, "Physical And Optical Properties Of Rare Earth Cobalt Materials", Nucl. Instr. and Meth. 187 (1981) 109.

where $\sigma_m = \frac{1}{\mu_0}\mathbf{B}_r \cdot \widehat{n}$, where $\widehat{n}$ is the unit vector normal to the block, pointing out of the block.

Using the volume charge density inside the blocks and the surface charge density on the boundaries, the solution for ϕ_m is

$$\phi_m(\mathbf{x}) = \frac{1}{4\pi}\int \frac{\rho_m(\mathbf{x}')}{|\mathbf{x}'-\mathbf{x}|}dV' + \frac{1}{4\pi}\int \frac{\sigma_m(\mathbf{x}')}{|\mathbf{x}'-\mathbf{x}|}dA' \tag{14}$$

The field $\mathbf{H} = -\nabla\phi_m$ has the following form.

$$\mathbf{H}(\mathbf{x}) = -\frac{1}{4\pi}\int \rho_m(\mathbf{x}')\frac{\mathbf{x}'-\mathbf{x}}{|\mathbf{x}'-\mathbf{x}|^3}dV' - \frac{1}{4\pi}\int \sigma_m(\mathbf{x}')\frac{\mathbf{x}'-\mathbf{x}}{|\mathbf{x}'-\mathbf{x}|^3}dA' \tag{15}$$

or

$$\mathbf{H}(\mathbf{x}) = \frac{1}{4\pi}\int \rho_m(\mathbf{x}')\frac{\mathbf{x}-\mathbf{x}'}{|\mathbf{x}-\mathbf{x}'|^3}dV' + \frac{1}{4\pi}\int \sigma_m(\mathbf{x}')\frac{\mathbf{x}-\mathbf{x}'}{|\mathbf{x}-\mathbf{x}'|^3}dA' \tag{16}$$

If we assume the blocks have uniform magnetization, then $\rho_m = 0$ inside the blocks. The field is now

$$\mathbf{H}(\mathbf{x}) = \frac{1}{4\pi}\int \sigma_m(\mathbf{x}')\frac{\mathbf{x}-\mathbf{x}'}{|\mathbf{x}-\mathbf{x}'|^3}dA' \tag{17}$$

or

$$\mathbf{H}(\mathbf{x}) = \frac{1}{4\pi}\int \frac{1}{\mu_0}\left[\mathbf{B}_r(\mathbf{x}')\cdot\widehat{n}(\mathbf{x}')\right]\frac{\mathbf{x}-\mathbf{x}'}{|\mathbf{x}-\mathbf{x}'|^3}dA' \tag{18}$$

$$\mathbf{B}(\mathbf{x}) = \frac{1}{4\pi}\int \left[\mathbf{B}_r(\mathbf{x}')\cdot\widehat{n}(\mathbf{x}')\right]\frac{\mathbf{x}-\mathbf{x}'}{|\mathbf{x}-\mathbf{x}'|^3}dA' \tag{19}$$

These are the formulas which were used to calculate the fields from the PPM undulator blocks.

The field $\mathbf{B}(\mathbf{x})$ is calculated numerically by dividing the surface of each magnet block into area elements. The manufacturer specifies $\mathbf{B}_r$ for the block. $\mathbf{B}_r \cdot \widehat{n}$ is calculated at each area element and multiplied by the area of the element to get the equivalent magnetic charge.

$$q_i = \mathbf{B}_r \cdot \widehat{n}\, dA_i \tag{20}$$

The charges are multiplied by the spatial factor in equation 19 and summed to calculate the field.

$$\mathbf{B}(\mathbf{x}) = \frac{1}{4\pi}\sum_i q_i \frac{\mathbf{x}-\mathbf{x}_i}{|\mathbf{x}-\mathbf{x}_i|^3} \tag{21}$$

The sum is over all charges on each block, and all blocks in the undulator.

2.2 End Design

The undulator ends were designed to be steering free and give a centered trajectory along the input beam direction[4]. Unit permeability magnet blocks were assumed. Figure 1 shows a vertical cross section of the upper end of an undulator magnet assembly and a simplified form of the resulting horizontal trajectory. The trajectory has been simplified by modelling the effect of each vertically magnetized block as a kick (trajectory slope change) at the center of the block, and the effect of each horizontally magnetized block as a kick at each end of the block, with the kicks in opposite directions.

We begin by considering the effect of blocks in the center of the undulator. We take the horizontal and vertical blocks to have length l_b. For this analysis, the vertical blocks are divided in half. The

[4] R. Schlueter, S. Marks, and S. Prestemon, "Elliptically Polarizing Undulator End Designs", IEEE Trans. on App. Superconductivity, 16, June, 2006.

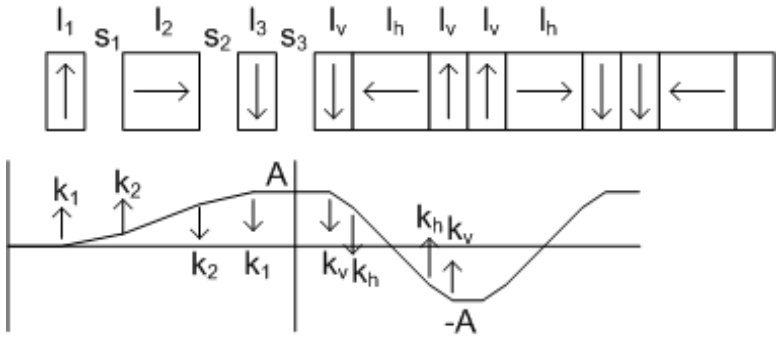

Figure 1: Vertical cross section of the end of the upper undulator magnet assembly and the approximate horizontal beam trajectory.

basic unit of the periodic structure is half a vertical block, followed by a horizontal block, followed by half a vertical block. The half vertical blocks have length $l_v = l_b/2$. The horizontal blocks have length $l_h = l_b$. This basic unit is steering free, i.e. it does not produce a net slope change. For every kick, there is an equal and opposite kick. When the incident slope is zero, the exit slope is zero. The basic unit takes the trajectory position from A in figure 1 to $-A$. A half vertical block changes the slope of the trajectory by k_v modeled as an impulse located at the center of the half block. Each end of a horizontal block changes the slope of the trajectory by k_h and the slope changes from the two ends have opposite sign. The second half vertical block in the basic unit changes the slope of the trajectory by $-k_v$. Given the slope changes and the lengths of the blocks, we calculate the trajectory change

$$2A = k_v \left(\frac{l_v}{2} + l_h + \frac{l_v}{2} \right) + k_h \left(l_h + \frac{l_v}{2} \right) - k_h \left(\frac{l_v}{2} \right) - k_v \left(0 \right) \tag{22}$$

Simplifying, we find

$$A = \frac{1}{2} k_v \left(l_v + l_h \right) + \frac{1}{2} k_h \left(l_h \right) \tag{23}$$

We now consider the blocks at the end of the undulator. The end magnets are numbered 1, 2, and 3. Their lengths are l_1, l_2, and l_3 as indicated in figure 1. The slope changes from end blocks are k_1 centered in the first block, k_2 and $-k_2$ at each end of the horizontal block, and $k_3 = -k_1$ to make the end magnets steering free. k_3 is centered in the third block. There is a space s_1 between blocks 1 and 2, space s_2 between blocks 2 and 3, and space s_3 between the end blocks and the undulator center blocks. The purpose of the three end blocks is to bring the trajectory to amplitude A with slope zero. This happens at the position of the center of the third block, so space s_3 has no impact on the design of the end. We take $s_3 = 0$ and in practice, combine block 3 with the first vertical half block of the center section. To reach amplitude A, we require

$$A = k_1 \left(\frac{l_1}{2} + s_1 + l_2 + s_2 + \frac{l_3}{2} \right) + k_2 \left(l_2 + s_2 + \frac{l_3}{2} \right) - k_2 \left(s_2 + \frac{l_3}{2} \right) - k_1 \left(0 \right) \tag{24}$$

In order to make $k_3 = -k_1$for blocks with the same magnetization, we require $l_3 = l_1$. Simplifying, we find

$$A = k_1 \left(l_1 + s_1 + l_2 + s_2 \right) + k_2 \left(l_2 \right) \tag{25}$$

We now equate the trajectory amplitude from the end blocks to the trajectory amplitude in the undulator center. This determines a relation between the end blocks and the center blocks.

$$k_1 (l_1 + s_1 + l_2 + s_2) + k_2 (l_2) = \frac{1}{2} k_v (l_v + l_h) + \frac{1}{2} k_h (l_h) \tag{26}$$

The slope changes from the vertical and horizontal blocks depend on block dimensions in different ways. In order for this equation to be always valid, we break this equation into two equations, one for the horizontal blocks and one for the vertical blocks.

$$k_2 (l_2) = \frac{1}{2} k_h (l_h) \tag{27}$$

$$k_1 (l_1 + s_1 + l_2 + s_2) = \frac{1}{2} k_v (l_v + l_h) \tag{28}$$

The slope change from the horizontal blocks depends on the block's transverse dimensions and not on its length, i.e. it depends on the magnetic charge at the ends of the block. We want all blocks to have the same transverse dimensions and same B_r, so $k_2 = k_h$. Equation 27 then gives

$$l_2 = \frac{1}{2} l_h \tag{29}$$

The slope change from a vertical block depends on the length of the block since its magnetic charges are along the beam direction. Let α be the proportionality factor between slope change and block length. We assume α is the same for all blocks since we require all blocks to have the same B_r. Then $k_1 = \alpha l_1$ and $k_v = \alpha l_v$. Setting $l_2 = l_h/2$, $l_h = l_b$, and $l_v = l_b/2$, the equation for the vertical blocks becomes

$$l_1 \left(l_1 + s_1 + \frac{l_b}{2} + s_2 \right) = \frac{1}{4} l_b \left(\frac{3}{2} l_b \right) \tag{30}$$

Since l_1, s_1, and s_2 are free parameters, there is some freedom in their choice. We choose $l_1 = l_b/4$, and $s_1 = s_2 = s$. Then

$$\frac{1}{4} l_b \left(\frac{3}{4} l_b + 2s \right) = \frac{1}{4} l_b \left(\frac{3}{2} l_b \right) \tag{31}$$

This gives

$$s = \frac{3}{8} l_b \tag{32}$$

The end design parameters are now all determined. In summary, all blocks have the same transverse dimensions, same B_r, and obey the following relations

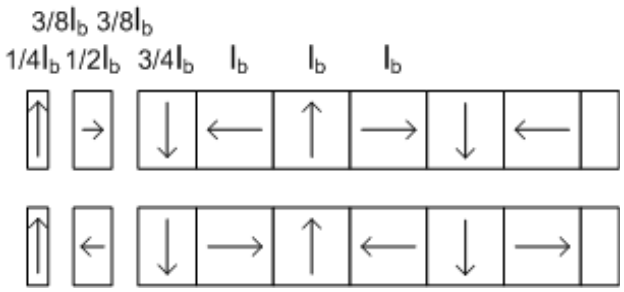

Figure 2: Design of the undulator ends.

$$l_1 = \frac{1}{4} l_b \tag{33}$$

$$l_2 = \frac{1}{2} l_b \tag{34}$$

$$l_3 = \frac{1}{4} l_b \tag{35}$$

$$s_1 = \frac{3}{8} l_b \tag{36}$$

$$s_2 = \frac{3}{8} l_b \tag{37}$$

$$s_3 = 0 \tag{38}$$

$$l_v = \frac{1}{2} l_b \tag{39}$$

$$l_h = l_b \tag{40}$$

In these equations, the center block length l_b is one quarter of the undulator period.

$$l_b = \frac{1}{4} \lambda_u \tag{41}$$

It should be noted that the vertical half blocks in the design above come in pairs, so in the actual construction, the vertical blocks have the same length as the horizontal blocks. The undulator end design is summarized in figure 2.

2.3 Force Calculations

The force on a magnet array is calculated by integrating the stress tensor over a surface enclosing the magnet array. Figure 3 shows a convenient surface for calculating the force on the lower magnet array. We take the surface outside the undulator at infinity where the fields are zero. The i'th component of the force is given by

$$F_i = \oint dS_j \frac{1}{\mu_0} \left(B_i B_j - \frac{1}{2} \delta_{ij} B_k B_k \right) \tag{42}$$

where i, j, k indicate the 1, 2, or 3 (x, y, or z) directions. We take z along the undulator, y is up, and x is along the width of the undulator. We approximate the surface integral in the gap by using the field along the axis of the undulator, the ($x = 0$, $y = 0$) line, and assuming the field is uniform in the x direction over the width of the magnets W. In the gap the surface element has

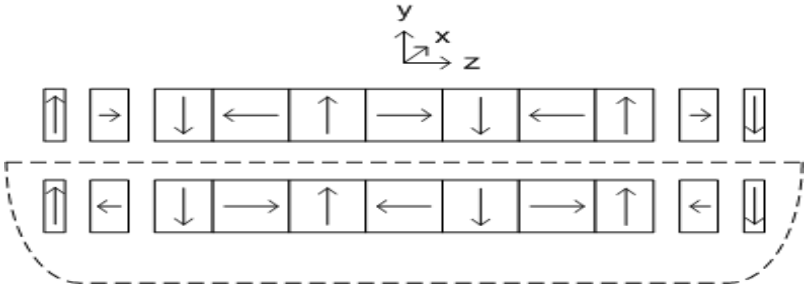

Figure 3: The force on the lower magnet array is calulcated by integrating the stress tensor over a surface enclosing the array.

one component in the y-direction: $dS_2 = Wdz$. The force components on the lower magnet array are then

$$F_x = \frac{W}{\mu_0}\int B_x B_y dz \tag{43}$$

$$F_y = \frac{W}{2\mu_0}\int \left(B_y^2 - B_z^2\right) dz \tag{44}$$

$$F_z = \frac{W}{\mu_0}\int B_z B_y dz \tag{45}$$

Numerical integration of the calculated fields in these equations gives the forces.

2.4 Trajectories, Phase, K Value, etc.

Once the fields along the axis of the undulator are calculated, the trajectories, phase, K value, etc. can be calculated. A separate analysis program was used to do the calculations. A version of the program for 2-D fields (B_x, B_y) was described in a previous note[5]. A new program was written to include 3-D fields for use in elliptically polarizing undulators (EPUs) and variable phase undulators. The B_z field component is large in these undulators and potentially produces second order effects on the trajectories.

The equation of motion for a relativistic electron in a magnetic field is

$$\frac{d}{dt}\left(\gamma m \mathbf{v}\right) = q\mathbf{v}\times\mathbf{B} \tag{46}$$

In this equation $\gamma = \frac{1}{\sqrt{1-(v/c)^2}}$ is the Lorentz factor, m is the electron rest mass, $\mathbf{v}$ is the electron velocity with magnitude v, q is the electron charge (q is negative), and $\mathbf{B}$ is the magnetic field strength. Since the energy of the electron is not changed by the magnetic field, γ is constant (we neglect the energy losses due to radiation) and can be taken outside the time derivative. The equation of motion becomes

$$\frac{d}{dt}\mathbf{v} = \frac{q}{\gamma m}\mathbf{v}\times\mathbf{B} \tag{47}$$

The time derivative is related to the derivative along the undulator by $\frac{d}{dt} = \frac{dz}{dt}\frac{d}{dz} = v_z\frac{d}{dz}$. The equation of motion can then be expressed as

[5] Z. Wolf, "Introduction To LCLS Undulator Tuning", LCLS-TN-04-7, June, 2004.

$$\frac{d}{dz}\mathbf{v} = \frac{q}{\gamma m v_z}\mathbf{v} \times \mathbf{B} \tag{48}$$

In component form the equation becomes

$$\frac{d}{dz}v_x = \frac{q}{\gamma m v_z}(v_y B_z - v_z B_y) \tag{49}$$

$$\frac{d}{dz}v_y = \frac{q}{\gamma m v_z}(v_z B_x - v_x B_z) \tag{50}$$

$$\frac{d}{dz}v_z = \frac{q}{\gamma m v_z}(v_x B_y - v_y B_x) \tag{51}$$

In the analysis program these equations are integrated numerically with initial conditions $v_x = 0$, $v_y = 0$, and $v_z = c\sqrt{1 - 1/\gamma^2}$,where $\gamma = E/mc^2$ is a constant with E being the electron energy.

Once the velocities are known, the transverse position of the electron at given z is calculated by numerically integrating the following equations.

$$\frac{d}{dz}x = \frac{v_x}{v_z} \tag{52}$$

$$\frac{d}{dz}y = \frac{v_y}{v_z} \tag{53}$$

Knowing the velocity and position of the electron, the slippage, phase, K value, etc. can be calculated. The slippage is the distance between a light wave and the electron. The slippage S changes according to

$$dS = (c - v_z)dt \tag{54}$$

or

$$dS = (\frac{c}{v_z} - 1)dz \tag{55}$$

Since we know v_z as a function of z, the slippage along the undulator is calculated by numerical integration.

The phase is given by dividing the slippage by λ_r and multiplying by 2π.

$$P(z) = \frac{2\pi S(z)}{\lambda_r} \tag{56}$$

The radiation wavelength λ_r is given by

$$\lambda_r = \frac{\lambda_u}{2\gamma^2}(1 + \frac{1}{2}K^2) \tag{57}$$

K is calculated by fitting a line to the slippage as a function of z. The slope of the fit, M_{fit}, gives K according to

$$M_{fit} = \frac{1}{2\gamma^2}(1 + \frac{1}{2}K^2) \tag{58}$$

$$K = \sqrt{2(2\gamma^2 M_{fit} - 1)} \tag{59}$$

2.5 Analytical Analysis

In order to gain insight into electron motion in the undulator, we now perform an analytical analysis pertaining to the center of an undulator with wide poles. The equations describing the magnetic field above and below a magnet array are $\nabla \times \mathbf{B} = 0$ and $\nabla \cdot \mathbf{B} = 0$. For for the 2-D case, $B_x = 0$ and these equations become $\partial_y B_z - \partial_z B_y = 0$ and $\partial_y B_y + \partial_z B_z = 0$. When the fields are expanded in a Fourier series, these equations have the following solutions. The fields above a magnet array are

$$B_y = \sum_{n=1}^{\infty} \beta_n \exp(-nk_u y) \cos(nk_u z + \psi_n) \tag{60}$$

$$B_z = \sum_{n=1}^{\infty} \beta_n \exp(-nk_u y) \sin(nk_u z + \psi_n) \tag{61}$$

The fields below a magnet array are

$$B_y = \sum_{n=1}^{\infty} \alpha_n \exp(nk_u y) \cos(nk_u z + \phi_n) \tag{62}$$

$$B_z = \sum_{n=1}^{\infty} -\alpha_n \exp(nk_u y) \sin(nk_u z + \phi_n) \tag{63}$$

We use these expressions for the fields to find the field in a variable phase undulator. We first look at the midplane at zero phase where $B_z = 0$. This implies $\alpha_n = \beta_n$ and $\phi_n = \psi_n$. We set $\phi_n = \psi_n = 0$, since a global phase is the same as a shift of the coordinate system. We now shift the top row of magnets by replacing z by $z - z_0$ in the equations for the fields below a magnet array. We add these fields to the fields from the bottom array. The fields in the variable phase undulator are

$$B_y = \sum_{n=1}^{\infty} \alpha_n \left[\exp(nk_u y) \cos(nk_u (z - z_0)) + \exp(-nk_u y) \cos(nk_u z)\right] \tag{64}$$

$$B_z = \sum_{n=1}^{\infty} \alpha_n \left[-\exp(nk_u y) \sin(nk_u (z - z_0)) + \exp(-nk_u y) \sin(nk_u z)\right] \tag{65}$$

Let $y = 0$ on the undulator midplane, and let B_n be the peak field on the midplane at zero undulator phase. Setting $y = 0$ and $z_0 = 0$ in the above expressions, we find $B_z = 0$ and the peak of the n'th harmonic of B_y is $2\alpha_n$, which we set equal to B_n. So $\alpha_n = B_n/2$. This gives the following expansion of the fields.

$$B_y = \frac{1}{2} \sum_{n=1}^{\infty} B_n \left[\exp(nk_u y) \cos(nk_u (z - z_0)) + \exp(-nk_u y) \cos(nk_u z)\right] \tag{66}$$

$$B_z = \frac{1}{2} \sum_{n=1}^{\infty} B_n \left[-\exp(nk_u y) \sin(nk_u (z - z_0)) + \exp(-nk_u y) \sin(nk_u z)\right] \tag{67}$$

We now use these fields to calculate the beam trajectory. Consider only the fundamental term with $n = 1$, and assume v_z is constant. We work to first order and neglect v_y when calculating v_x. With these assumptions, the equation for v_x is

$$\frac{d}{dz} v_x = -\frac{q}{\gamma m} B_y \tag{68}$$

Integrating, we find

$$v_x = -\frac{q}{2\gamma m k_u} B_1 \left[\exp\left(k_u y\right) \sin\left(k_u \left(z - z_0\right)\right) + \exp\left(-k_u y\right) \sin\left(k_u z\right)\right] \tag{69}$$

A constant of integration has been neglected since we are only interested in the oscillating velocity in the center of the undulator.

Using v_x, we can now calculate v_y. The equation for v_y with the assumptions given above is

$$\frac{d}{dz} v_y = -\frac{q}{\gamma m v_z} v_x B_z \tag{70}$$

Keeping v_z constant and inserting the expressions for v_x and B_z, we find

$$\begin{aligned} \frac{d}{dz} v_y = -\frac{q}{\gamma m v_z} &\left(-\frac{q}{2\gamma m k_u} B_1 \left[\exp\left(k_u y\right) \sin\left(k_u \left(z - z_0\right)\right) + \exp\left(-k_u y\right) \sin\left(k_u z\right)\right]\right) \\ &\times \left(\frac{1}{2} B_1 \left[-\exp\left(k_u y\right) \sin\left(k_u \left(z - z_0\right)\right) + \exp\left(-k_u y\right) \sin\left(k_u z\right)\right]\right) \end{aligned} \tag{71}$$

or

$$\frac{d}{dz} v_y = \frac{q^2 B_1^2}{4\gamma^2 m^2 v_z k_u} \left[-\exp\left(2k_u y\right) \sin^2\left(k_u \left(z - z_0\right)\right) + \exp\left(-2k_u y\right) \sin^2\left(k_u z\right)\right] \tag{72}$$

Averaging along z, we find

$$\left\langle \frac{d}{dz} v_y \right\rangle = -\frac{q^2 B_1^2}{4\gamma^2 m^2 v_z k_u} \sinh\left(2k_u y\right) \tag{73}$$

The average vertical velocity is

$$\langle v_y \rangle = -\frac{q^2 B_1^2}{4\gamma^2 m^2 v_z k_u} \sinh\left(2k_u y\right) z \tag{74}$$

where $v_y = 0$ at $z = 0$ has been assumed. The average vertical position is

$$\langle y \rangle = -\frac{q^2 B_1^2}{8\gamma^2 m^2 v_z^2 k_u} \sinh\left(2k_u y\right) z^2 \tag{75}$$

where we have assumed $y = 0$ at $z = 0$. These equations represent standard undulator focusing. A particle above the midplane has a downward force. A particle below the midplane has an upward force. A particle on the midplane has $\left\langle \frac{d}{dz} v_y \right\rangle = 0$. There is no net vertical force on a particle on the midplane in the body of a variable phase undulator. A particle which gets an initial v_y from the end of the undulator, keeps the same v_y through the entire undulator. We will come back to this when we see below that the vertical trajectory of a particle on the midplane has a nonzero slope in the center of the undulator.

3 Results

The numerical methods outlined above were used to model a variable phase undulator, calculate its field on the axis, calculate the forces, and calculate the beam trajectories, phase, and other undulator parameters. The model undulator used blocks which had the same transverse dimensions as the LCLS-I magnet blocks: 57.0 mm high by 66.0 mm wide. The period of the undulator was the same as for LCLS-I, 30 mm, and each block in the pure permanent magnet model had a thickness of one quarter the period, i.e. the blocks were 7.5 mm thick. The gap of the model undulator was varied, but for most calculations was set to the nominal LCLS-I undulator gap of 6.8 mm. The bottom row of magnets was fixed in the model and the top row moved longitudinally to vary the phase. The remnant field in the magnet blocks was taken to be 1.2 T.

3.1 K vs Gap

Figure 4 shows how the K value of the undulator changes with gap over a gap range of 6.5 to 7.2 mm. The phase is set to zero for the figure. At 6.8 mm, the peak B field has a value of 1.051 T,

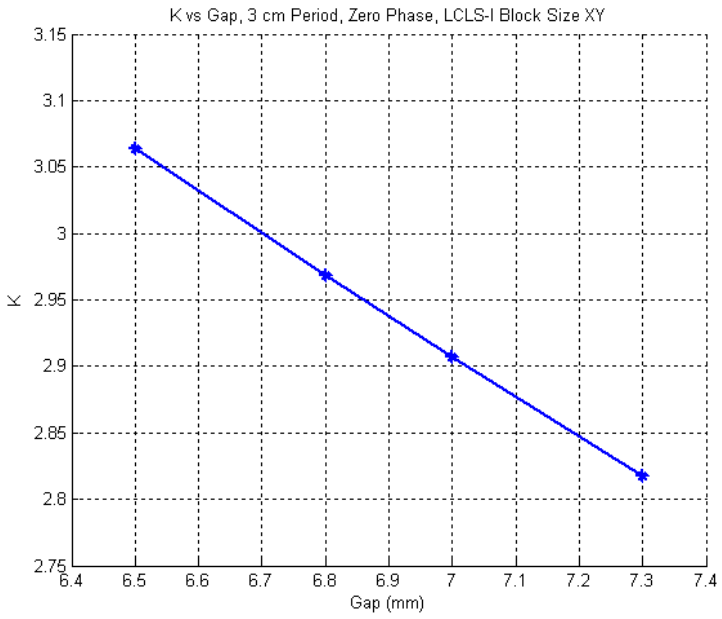

Figure 4: This figure shows how the K value of the undulator changes with gap. The phase was set to zero.

and the K value is 2.969.

Halbach studied PPM undulators in a paper[6] in which he gave the plot shown in figure 5 which gives the peak field as a function of g/λ. The plot was calculated using the following equation.

$$B_z - iB_y = i1.723B_r \exp\left(-\frac{\pi g}{\lambda}\right) \cos\left[\frac{2\pi}{\lambda}(z+iy)\right] \tag{76}$$

This equation assumes a magnet block height of $\lambda/2 = 15$ mm, which is significantly different than the 57 mm block height we are using. Note that the figure also used a remnant field of $B_r = 0.9$ T. The model undulator presented here has $g/\lambda = 0.227$ when $g = 6.8$ mm and $\lambda = 30$ mm. Using the formula with $B_r = 1.2$ T and $y = 0$, we find a peak field of $B_y = 1.013$ T. This does not agree well with the peak field from the model due to the block height difference.

A more general equation is given in another Halbach paper[7]. The equation is

$$B_z - iB_y = i2B_r \sum_{\nu=0}^{\infty} \cos(nk\varsigma) \exp(-nkh)(1 - \exp(-nkL)) \sin\left(\frac{n\epsilon\pi}{M}\right) / \left(\frac{n\pi}{M}\right) \tag{77}$$

where $n = 1 + \nu M$, $k = 2\pi/\lambda$, $\varsigma = z + iy$, M is the number of blocks per period which is 4 in our case, $h = g/2$, L is the block height which is 57 mm in our case, ϵ is the longitudinal fraction of the

[6] K. Halbach, "Permanent Magnet Undulators", Journal De Physique C1 (1983) 211.

[7] K. Halbach, "Physical And Optical Properties Of Rare Earth Cobalt Materials", Nucl. Instr. and Meth. 187 (1981) 109.

undulator occupied by magnets which is 1 in our case. Using these parameters and including up to the 10'th harmonic, this equation gives a peak field of 1.048 T and a K value of 2.970. This is much closer to the charge model value of 1.051 T for the peak field and $K = 2.969$. Note that the harmonics affect the peak field much more strongly than the K value.

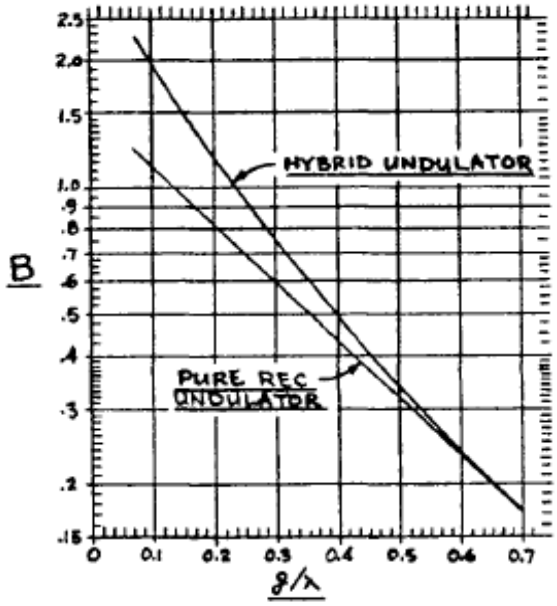

Fig. 3. Peak Midplane Fields in Hybrid and Pure REC Undulators

Figure 5: Halbach calculated the peak fields of PPM and hybrid undulators.

3.2 K vs Phase

Figure 6 shows the variation of the K value as the top magnet assembly is moved longitudinally past the bottom assembly. A gap of 6.8 mm was used in this figure. The K value changes smoothly from a peak value of 2.969 at zero shift, to $K = 0$ at a shift of $\lambda_u/2$.

We wish to know how accurately the top magnet assembly must be positioned in order to achieve a certain K value within $dK/K = 1 \times 10^{-4}$. Since the undulator period is 0.03 m, the phase in figure 6 can be converted into distance the top magnet assembly has moved ξ. The sensitivity of K to magnet assembly motion, $dK/d\xi$, varies from approximately 0 at zero phase to 309 1/m at a phase of $\lambda_u/2$. At $K = 2.46$, the fourth point from the left, the sensitivity $dK/d\xi = 197$ 1/m. Using this sensitivity, in order to set K to 2.46×10^{-4} requires the longitudinal position of the magnet assembly be set to $d\xi = 1.25 \times 10^{-6}$ m. This is similar to the accuracy required when setting the gap of an adjustable gap undulator. Only if the variable phase undulator is operated near maximum K is the positioning accuracy of the magnet assembly reduced.

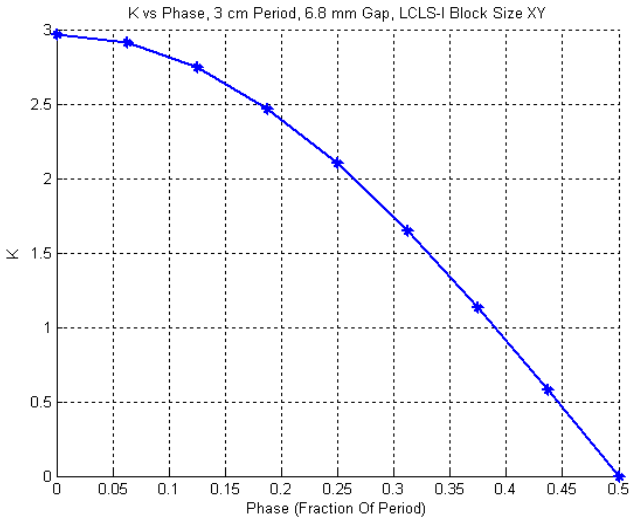

Figure 6: Variation of the K value as a function of the distance the top row of magnets is moved, expressed as a fraction of the undulator period.

3.3 Beam Trajectories

Figure 7 shows the magnetic field on the undulator axis when the top row of magnets is shifted longitudinally by 3/8 of the undulator period. A large longitudinal field B_z is introduced on the axis by the shift. We wish to know if this large B_z field affects the beam trajectories.

Figure 8 shows the x and y trajectories at a beam energy of 13.6 Gev, with the top row of magnets shifted by 3/8 of the undulator period. The beam entered on the undulator axis at x=0 and y=0. No steering or offset from the undulator ends is visible at this energy. No effect from B_z is visible either.

Figure 9 shows the x and y trajectories when the beam energy is 4.2 GeV. At this lower energy, a small amount of vertical steering in the ends is visible. At zero phase, there is no vertical steering, so the effect does not come from the undulator end design. As the phase increases, the slope of the vertical trajectory increases. The maximum slope is approximately $dy/dz = 5.07 \times 10^{-8}$. The vertical trajectory slope as a function of phase is shown in figure 10 with a beam energy of 4.2 GeV. The fields at the end of the undulator change with phase. The beam receives an initial vertical kick with non-zero phase which causes a constant vertical velocity, or constant trajectory slope in the center of the undulator. The slope increases as the phase increases.

When the beam enters the undulator above the midplane, it is deflected downward due to undulator focusing. Figure 11 shows the x and y trajectories when the beam enters the undulator 200 μm above the midplane. The figure shows the trajectories relative to the incident position. The undulator phase shift is 3/8 λ_u in this figure. When the beam enters at $x = 0$ and $y = -200$ μm, the trajectories in figure 12 result. Again the phase shift is 3/8 λ_u.

The beam position at the end of the undulator is given by equation 75. Inserting appropriate values for the quantities, for an incident beam 200 μm off the midplane, equation 75 gives an exit y-position offset by 1.15 μm from the entrance position. This agrees fairly well with the previous two figures at the undulator end which is at $z = 1.01$ m. The absolute values of the exit positions are different in the two figures. This is due to the vertical slope of the trajectory due to the phase shift as seen earlier. At zero phase, the absolute values of the beam exit positions are the same, and in good agreement with the undulator focusing formula. In summary, undulator focusing is

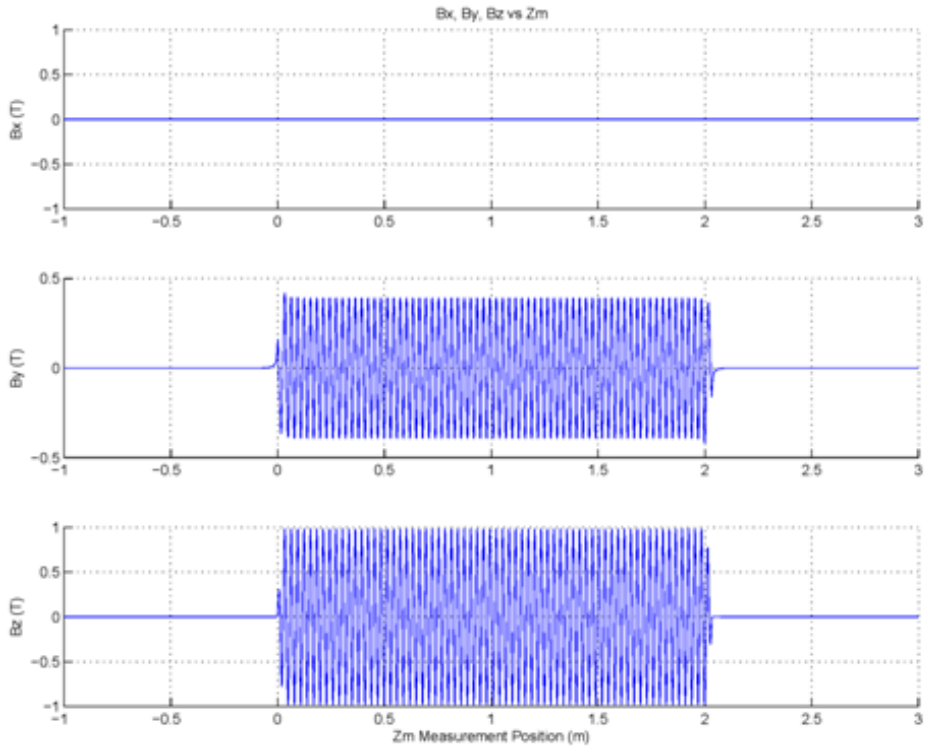

Figure 7: Magnetic field components B_x, B_y, and B_z on the undulator axis when the top row of magnets are shifted by 3/8 of the undulator period relative to the bottom row.

observed in variable phase undulators, in addition to the slope of the vertical trajectory due to the initial kick of the beam at the entrance. More importantly, there appears to be no anomalous behavior of the beam when it is offset from the midplane.

3.4 Force vs Phase

The forces between the upper and lower undulator halves change with phase. Figure 13 shows the force components per unit length as a function of phase. The force in the x-direction is zero. The vertical force goes from maximum attractive at zero phase, to zero at a phase of 0.25 λ_u, to maximum repulsive at a phase of 0.5 λ_u. The magnitude of the peak vertical force force is 2.95×10^4 N (6650 pounds) for the 2.02 m long undulator with a gap of 6.8 mm, which gives a force per unit length of 1.46×10^4 N/m.. The longitudinal force, F_z, goes from zero at zero phase, to a maximum of 2.95×10^4 N at a phase of 0.25 λ_u, to zero at a phase of 0.5 λ_u. The total force was divided by the undulator total length to get the force per unit length. End effects are included in the force per unit length calculation causing small changes as the undulator length is varied. More importantly, the fields were assumed to have an effective width in x equal to the width of the magnet blocks. This analysis gives an initial estimate of the forces, but more extensive 3-D calculations are required to design an undulator.

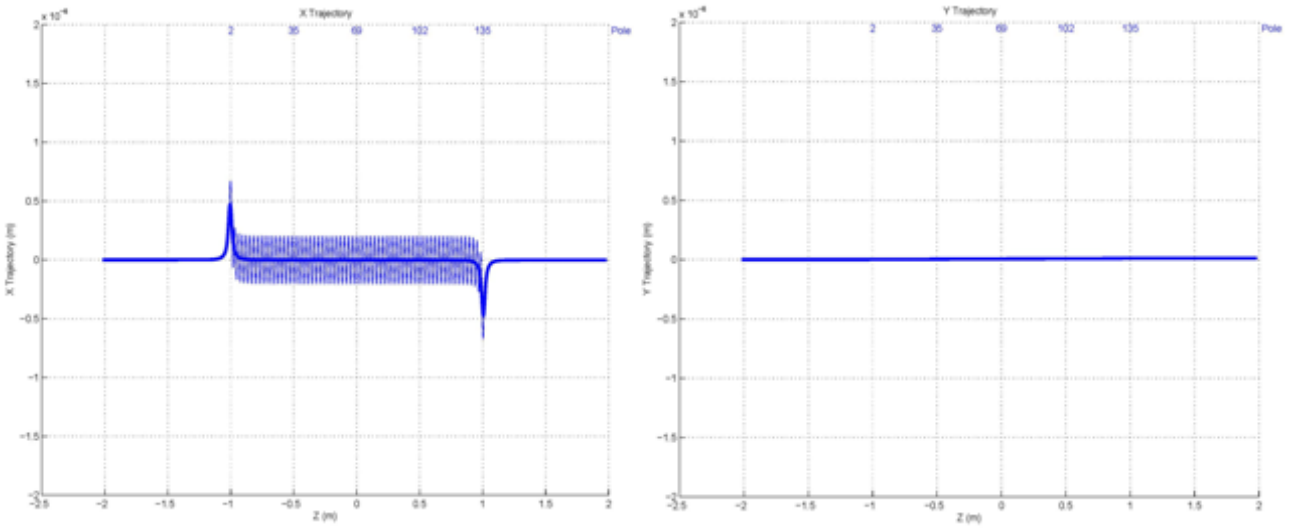

Figure 8: Beam trajectories at 13.6 Gev with the top row of magnets shifted by 3/8 of the undulator period. The beam entered on the undulator axis.

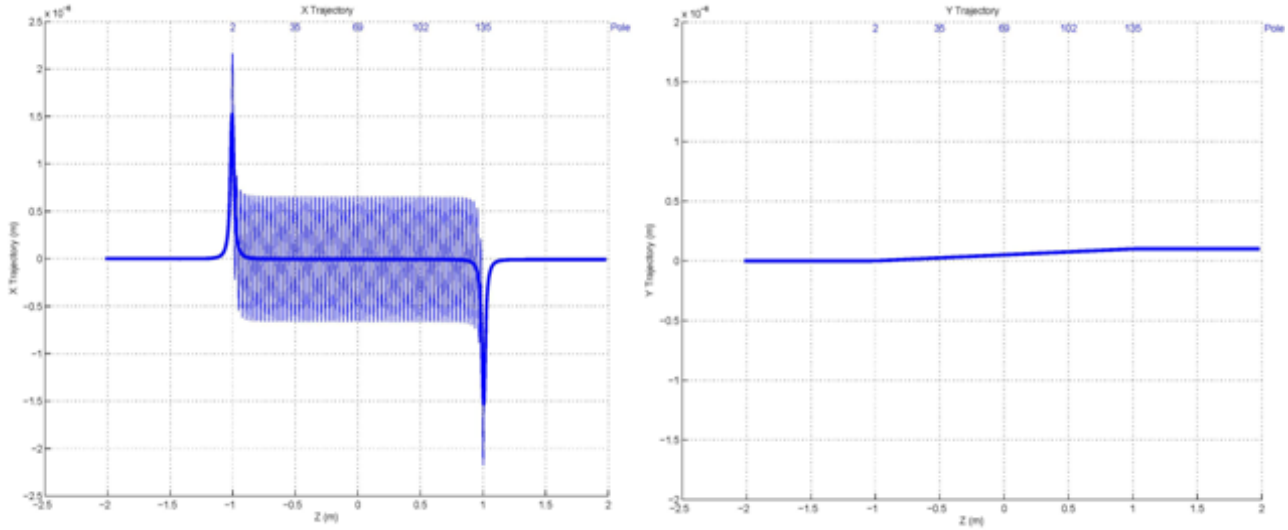

Figure 9: x and y trajectories for a beam energy of 4.2 GeV and the top row of magnets shifted by 3/8 of the undulator period. The beam entered on the undulator axis.

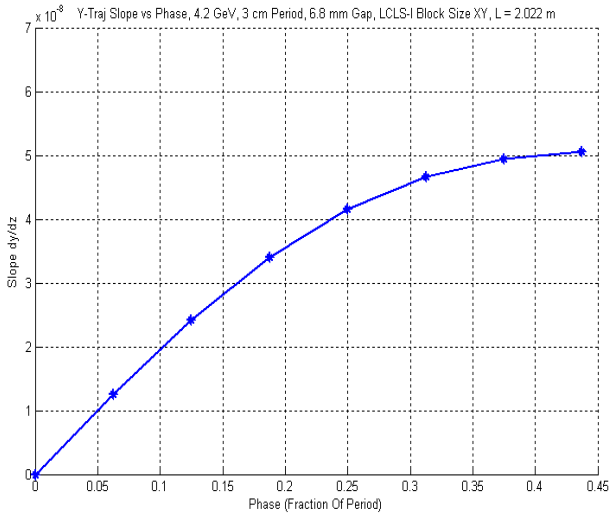

Figure 10: The slope of the vertical trajectory increases with phase to a peak value of approximately 5.07×10^{-8}. The slope is zero at zero phase, showing that the effect does not come from the end design.

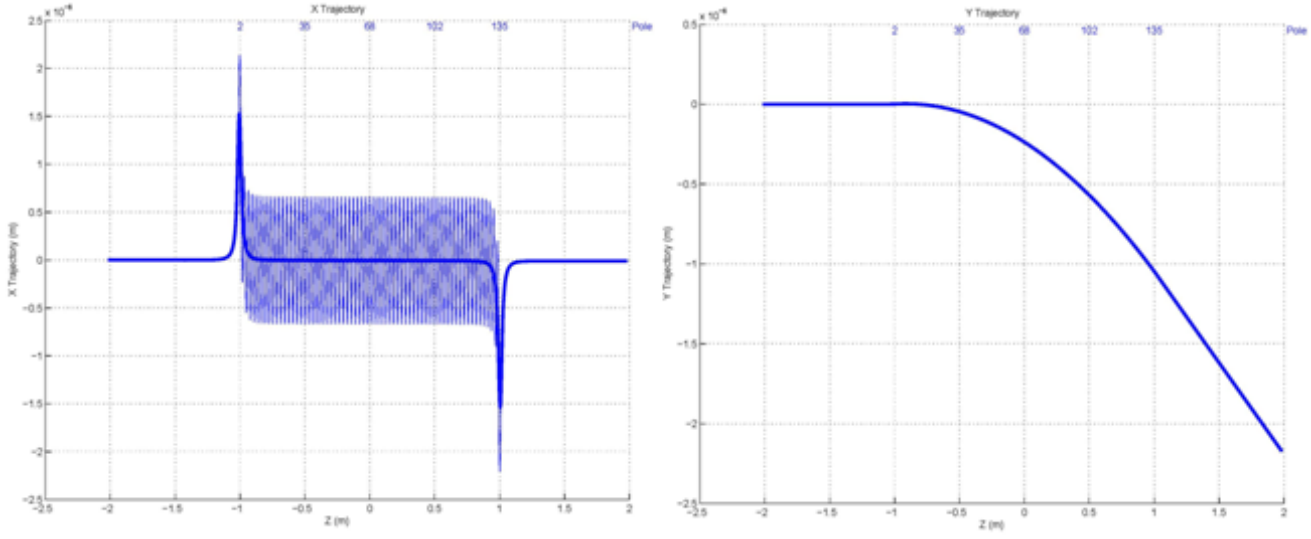

Figure 11: x and y trajectories when the beam energy is 4.2 GeV and when the beam enters the undulator 200 μm above the midplane.

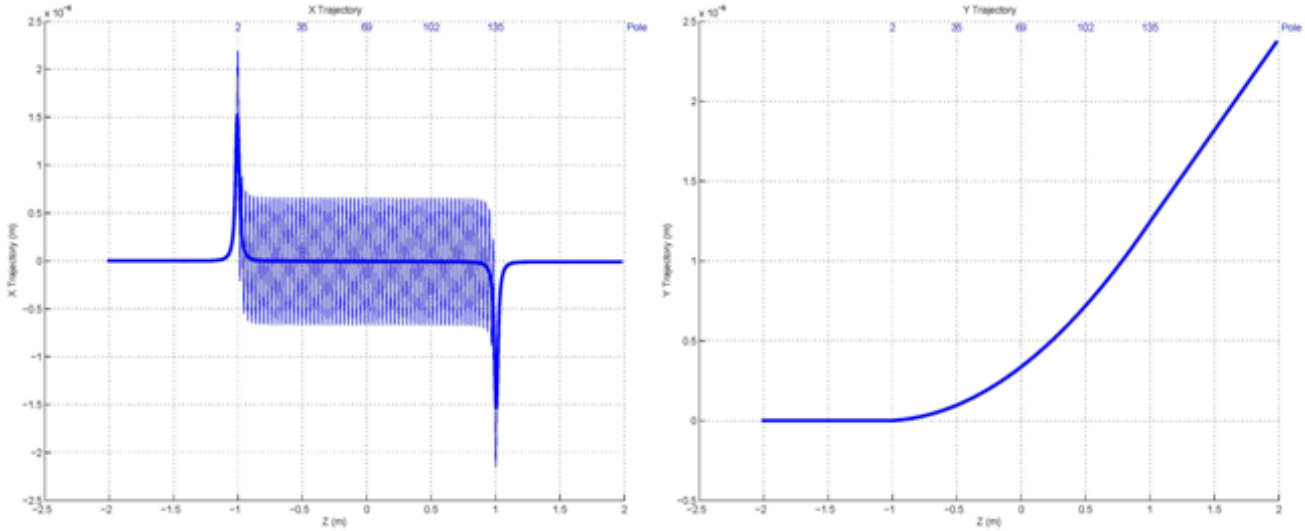

Figure 12: x and y trajectories when the 4.2 GeV beam enters the undulator at $x_0 = 0$ μm, $y_0 = -200$ μm. The trajectories shown are relative to the entrance position.

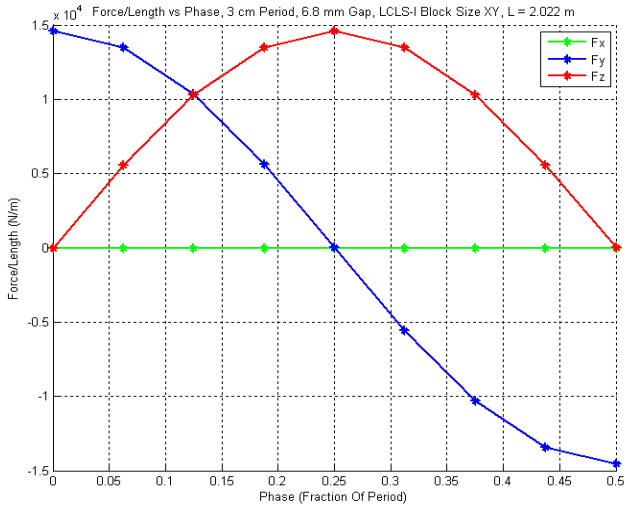

Figure 13: Force per unit length on the lower half of a 2.022 meter long undulator as a function of the shift of the upper magnet array expressed as a fraction of the undulator period. The gap is 6.8 mm.

4 Conclusion

A PPM variable phase undulator was studied. The undulator parameters were similar the LCLS-I undulator parameters. Several results are notable. Setting K precisely in a variable phase undulator requires similar mechanical accuracy as for an adjustable gap undulator. Trajectories in the variable phase undulator are similar to those in standard planar undulators, but there is a small vertical velocity component to the beam in the undulator. This comes from the shift of the magnet arrays at the entrance end. The exit end compensates for the slope change in the antisymmetric design which was studied. The resulting offset will probably need correction at low energies. A new feature of the design is the magnetic force behavior with phase. Vertical forces change sign from attractive to repulsive at the quarter period phase. Longitudinal forces peak at the quarter period phase and have a magnitude equal to the peak vertical force. The mechanical design of the undulator will need to account for these forces. The mechanical design will also need to keep the gap repeatable at the micron level as a function of phase in order to insure K repeatability to 10^{-4}.

Acknowledgements
I am grateful to Heinz-Dieter Nuhn for many discussions about this work.